Supplementary Materials for

Tailoring Electrical Transport Across Grain Boundaries in Polycrystalline Graphene

Adam W. Tsen, Lola Brown, Mark P. Levendorf, Fereshte Ghahari, Pinshane Y. Huang, Robin W. Havener, Carlos S. Ruiz-Vargas, David A. Muller, Philip Kim, Jiwoong Park*

*To whom correspondence should be addressed. E-mail: jpark@cornell.edu

Published 1 June 2012, *Science* **336**, 1143 (2012)
DOI: 10.1126/science.1218948

This PDF file includes:

Materials and Methods
Figs. S1 to S7
References

Materials and Methods

Synthesis of graphene with various domain size *D*:

All graphene is grown on 25 μm thick copper foil in a custom hot-wall quartz tube furnace at ≈2 Torr pressure using the process reported by Li *et al.* (*2*).

Growth A (*D* ≈1 μm): Copper substrates were heated to the reaction temperature of 1000 °C in a hydrogen environment (H_2: 100 sccm). After annealing for one hour, methane (CH_4: 6 sccm) was introduced. Following a 10 minute growth stage, the chamber was slowly cooled to room temperature.

Growth B (*D* ≈10 μm): Copper is heated to 1050 °C in a hydrogen environment (H_2:300 sccm) and annealed for 30 minutes. Methane (CH_4: 0.8 sccm) is introduced for 30 minutes for partial growth (Fig. S1, top) and 90 minutes for complete coverage. The furnace is subsequently cooled.

Growth C (*D* ≈50 μm): After Li *et al.* (*14*), a closed "pocket" made of copper foil was heated between 980-1000 °C in a hydrogen environment (H_2: 60-120 sccm) and annealed up to 3 hours. Methane (CH_4: 1 sccm) is introduced for 90 minutes for partial growth (Fig. S1, bottom) and ≈3 hours for complete coverage, after which the furnace is cooled.

Fabrication of transmission electron microscopy chip compatible with electrical measurements:

Here, we describe the fabrication of transmission electron microscopy (TEM) chips that are compatible with electron-beam lithography and electrical measurements. A completed chip is shown in figure S2 (A). It is 2.33 mm wide on each side, 200 μm thick, and fits standard holders. In the center is a fully suspended, silicon nitride (SiN) TEM window (80x80 μm, 20 nm thickness) with metalized alignment marks. On the periphery are large electrical leads and contacts. The chips are fabricated on the wafer scale using optical lithography and cleaved individually at the end. A schematic of the process flow is shown in figure S2 (B). First, we grow 50 nm of low stress SiN on 200 μm thick silicon (Si) <100> wafers. In two separate lithography steps we pattern and metalize alignment marks and electrical leads close to the TEM window (20 nm Cr/Au) as well as contact pads on the chip periphery (150 nm Cr/Au). Next, we pattern and etch large SiN windows on the backside of the chip using reactive ion etching (RIE) to allow for KOH etching of the Si substrate underlying the TEM window. After transferring graphene, the SiN TEM window is further thinned from the back to ≈20 nm with RIE.

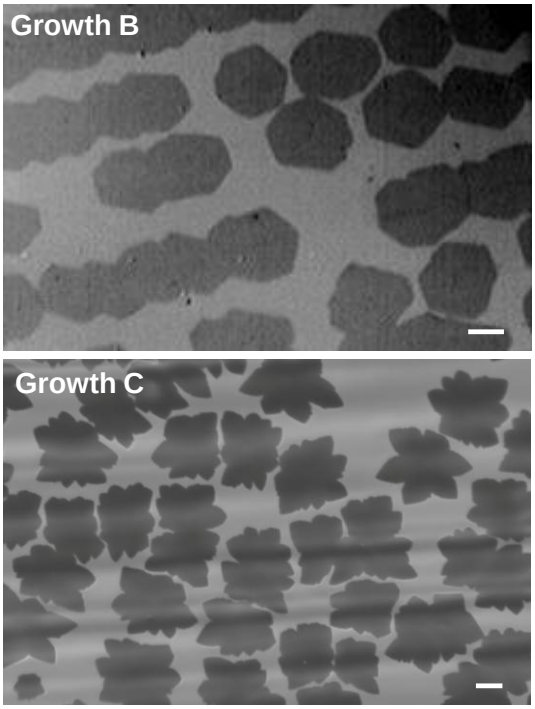

Fig. S1

Top: optical image of polygon graphene islands from growth B transferred onto SiO_2/Si. Bottom: optical image of flowered graphene islands from growth C on copper foil. Scale bars: 10 μm.

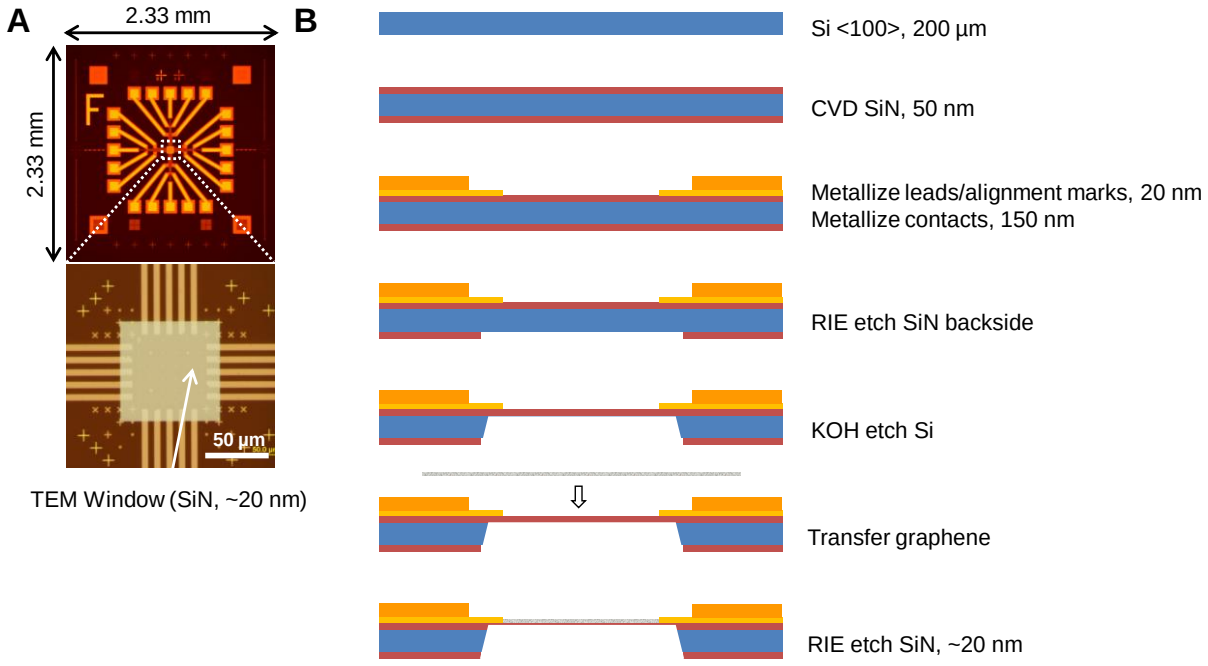

Fig. S2

(A) Optical images of completed TEM chip compatible with e-beam lithography and electrical measurements. **(B)** Schematic outlining fabrication procedure: 1) Grow 50 nm of SiN on 200 µm thickness Si wafer. 2) Metallize electrical contacts and leads. 3) RIE etch SiN windows on backside for 4) KOH etch of Si. After transferring graphene, 5) thin SiN TEM window to ≈20 nm from backside with RIE.

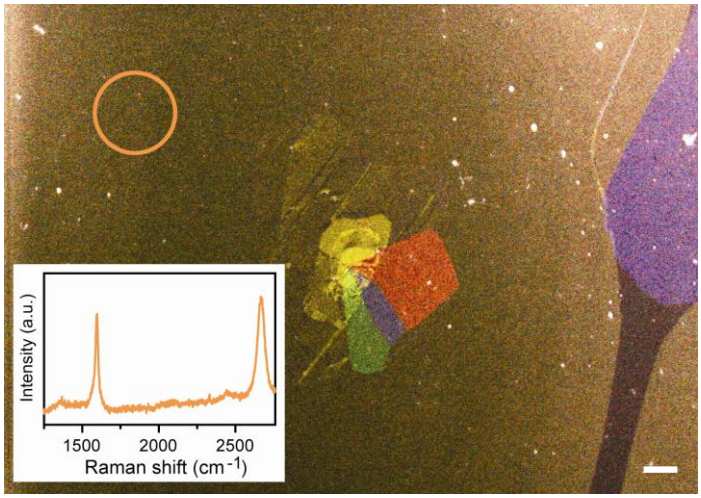

Fig. S3

Micro-Raman spectrum (inset) of graphene taken after dark-field TEM imaging (main panel). Small D peak shows minimal radiation damage in contrast with (*26*) and (*27*). Raman location is indicated by circle. Scale bar: 1 μm.

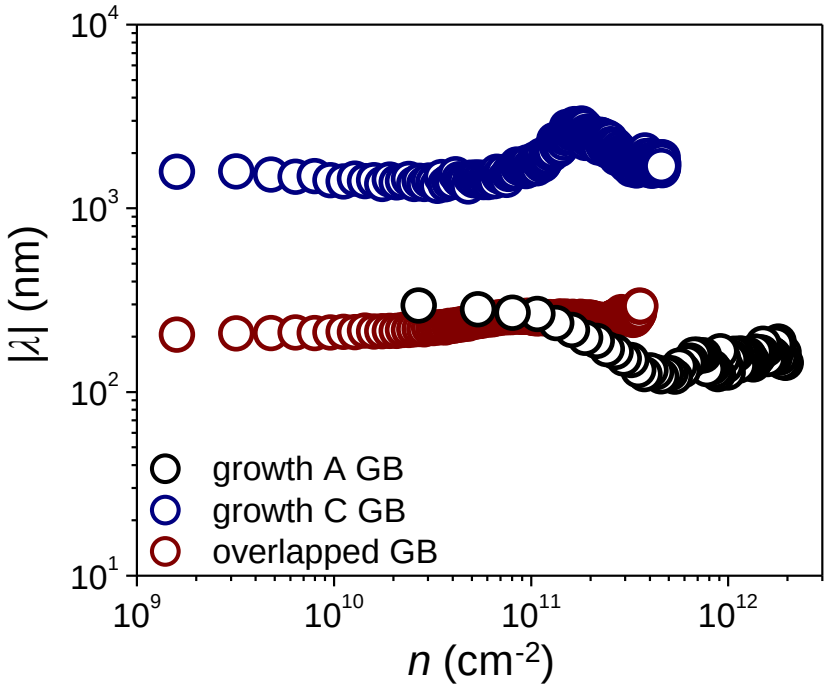

Fig. S4
Effective length $|\lambda|$ as function of hole density $n = C\,|V_G - V_{Dirac}|/e$ for devices shown in Fig. 2A, B, E. λ changes only within a factor of ≈2 as n is tuned by three orders of magnitude.

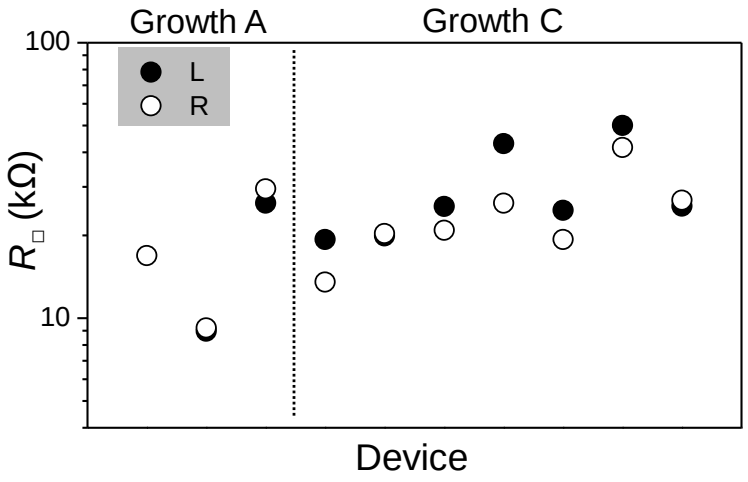

Fig. S5

Intra-domain sheet resistance (L, R) measured at the Dirac point for all TEM-resolved devices. No strong differences are seen between growths A and C.

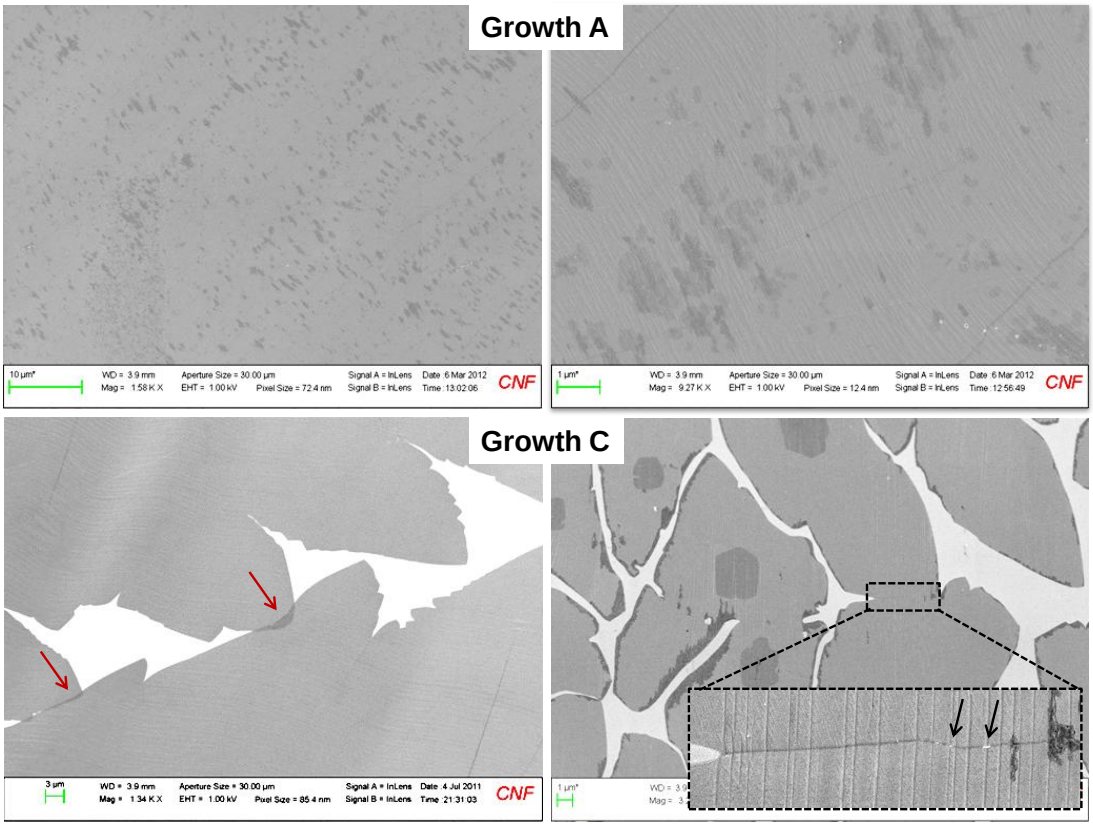

Fig. S6

Scanning electron micrographs of growths A (top) and C (bottom) on copper foil. Growth A completely covers copper surface, but growth C shows many areas with gaps and overlaps (denoted by red arrows), suggesting reduced tendency for inter-domain merging. Zoom-in image of area between islands shows dark line and small holes on boundary (denoted by black arrows).

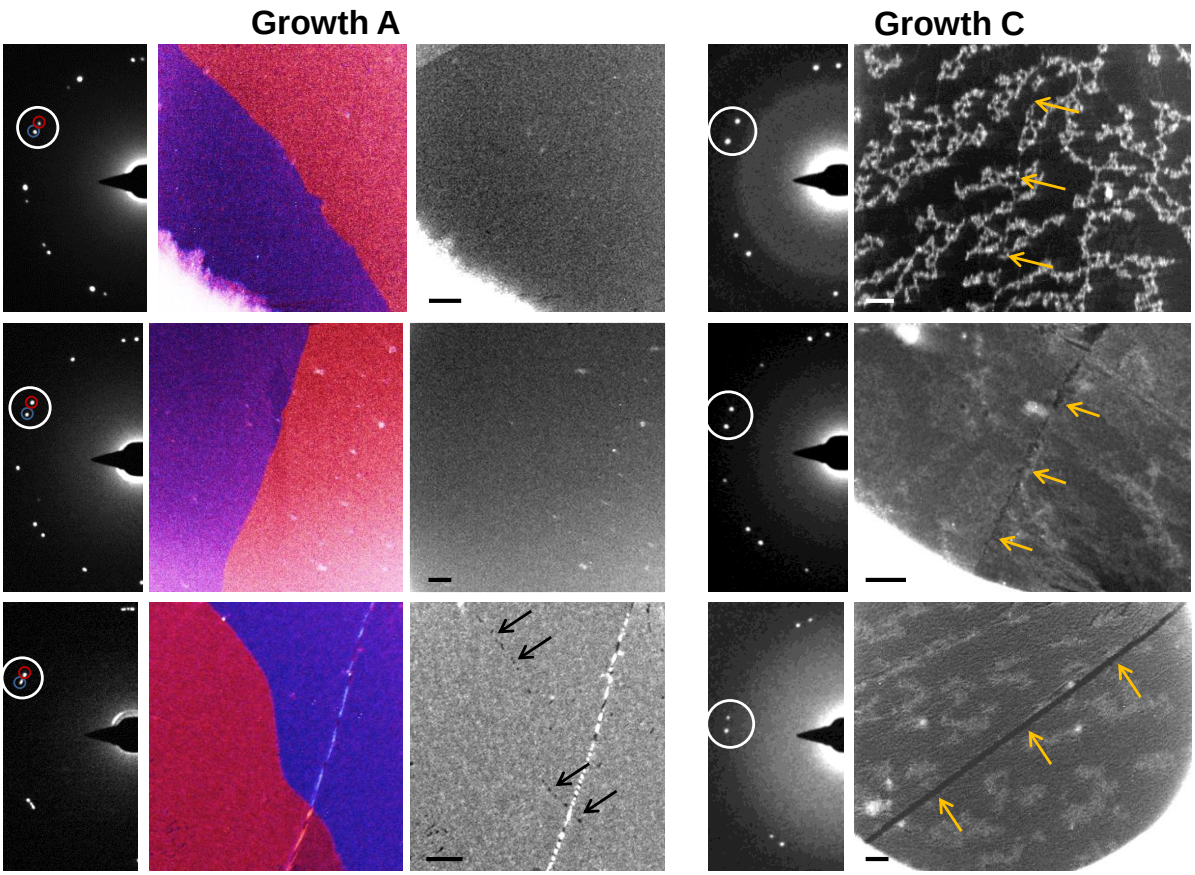

Fig. S7

Dark-field TEM images of individual grain boundaries from growths A (left) and C (right) suspended on holes. Diffraction spots and apertures used to form images are shown in insets. Domains from growth A almost always make seamless connections when selecting both spots simultaneously, although dark spots (denoted by black arrows) indicate imperfect stitching occasionally. Boundaries from growth C (denoted by gold arrows) are always visible with varying amounts of discontinuity.

References

1. D. B. Holt, B. G. Yacobi, *Extended Defects in Semiconductors: Electronic Properties, Device Effects and Structures* (Cambridge University Press, Cambridge; New York, 2007).

2. X. Li *et al*., Large-area synthesis of high-quality and uniform graphene films on copper foils. *Science* **324**, 1312 (2009). doi:10.1126/science.1171245 Medline

3. S. Bae *et al*., Roll-to-roll production of 30-inch graphene films for transparent electrodes. *Nat. Nanotechnol.* **5**, 574 (2010). doi:10.1038/nnano.2010.132 Medline

4. P. Y. Huang *et al*., Grains and grain boundaries in single-layer graphene atomic patchwork quilts. *Nature* **469**, 389 (2011). doi:10.1038/nature09718 Medline

5. K. Kim *et al*., Grain boundary mapping in polycrystalline graphene. *ACS Nano* **5**, 2142 (2011). doi:10.1021/nn1033423 Medline

6. O. V. Yazyev, S. G. Louie, Electronic transport in polycrystalline graphene. *Nat. Mater.* **9**, 806 (2010). doi:10.1038/nmat2830 Medline

7. O. V. Yazyev, S. G. Louie, Topological defects in graphene: Dislocations and grain boundaries. *Phys. Rev. B* **81**, 195420 (2010). doi:10.1103/PhysRevB.81.195420

8. A. Mesaros, S. Papanikolaou, C. F. J. Flipse, D. Sadri, J. Zaanen, Electronic states of graphene grain boundaries. *Phys. Rev. B* **82**, 205119 (2010). doi:10.1103/PhysRevB.82.205119

9. N. M. R. Peres, F. Guinea, A. H. Castro Neto, Electronic properties of disordered two-dimensional carbon. *Phys. Rev. B* **73**, 125411 (2006). doi:10.1103/PhysRevB.73.125411

10. X. Li *et al*., Graphene films with large domain size by a two-step chemical vapor deposition process. *Nano Lett.* **10**, 4328 (2010). doi:10.1021/nl101629g Medline

11. Q. Yu *et al*., Control and characterization of individual grains and grain boundaries in graphene grown by chemical vapour deposition. *Nat. Mater.* **10**, 443 (2011). doi:10.1038/nmat3010 Medline

12. L. A. Jauregui, H. Cao, W. Wu, Q. Yu, Y. P. Chen, Electronic properties of grains and grain boundaries in graphene grown by chemical vapor deposition. *Solid State Commun.* **151**, 1100 (2011). doi:10.1016/j.ssc.2011.05.023

13. Materials and methods are available as supplementary materials on *Science* Online.

14. X. Li *et al*., Large-area graphene single crystals grown by low-pressure chemical vapor deposition of methane on copper. *J. Am. Chem. Soc.* **133**, 2816 (2011). doi:10.1021/ja109793s Medline

15. A. W. Robertson *et al*., Atomic structure of interconnected few-layer graphene domains. *ACS Nano* **5**, 6610 (2011). doi:10.1021/nn202051g Medline

16. Y. W. Tan *et al*., Measurement of scattering rate and minimum conductivity in graphene. *Phys. Rev. Lett.* **99**, 246803 (2007). doi:10.1103/PhysRevLett.99.246803 Medline

17. N. H. Shon, T. Ando, Quantum transport in two-dimensional graphite system. *J. Phys. Soc. Jpn.* **67**, 2421 (1998). doi:10.1143/JPSJ.67.2421

18. S. Adam, E. H. Hwang, V. M. Galitski, S. Das Sarma, A self-consistent theory for graphene transport. *Proc. Natl. Acad. Sci. U.S.A.* **104**, 18392 (2007). doi:10.1073/pnas.0704772104 Medline

19. T. Stauber, N. M. R. Peres, F. Guinea, Electronic transport in graphene: A semiclassical approach including midgap states. *Phys. Rev. B* **76**, 205423 (2007). doi:10.1103/PhysRevB.76.205423

20. J.-H. Chen, W. G. Cullen, C. Jang, M. S. Fuhrer, E. D. Williams, Defect scattering in graphene. *Phys. Rev. Lett.* **102**, 236805 (2009). doi:10.1103/PhysRevLett.102.236805 Medline

21. Y. W. Tan, Y. Zhang, H. L. Stormer, P. Kim, Temperature dependent electron transport in graphene. *Eur. Phys. J. Spec. Top.* **148**, 15 (2007). doi:10.1140/epjst/e2007-00221-9

22. G.-X. Ni *et al*., Quasi-periodic nanoripples in graphene grown by chemical vapor deposition and its impact on charge transport. *ACS Nano* **6**, 1158 (2012). doi:10.1021/nn203775x Medline

23. C. R. Dean *et al*., Boron nitride substrates for high-quality graphene electronics. *Nat. Nanotechnol.* **5**, 722 (2010). doi:10.1038/nnano.2010.172 Medline

24. W. Gannett *et al*., Boron nitride substrates for high mobility chemical vapor deposited graphene. *Appl. Phys. Lett.* **98**, 242105 (2011). doi:10.1063/1.3599708

25. J. N. Coleman *et al*., Two-dimensional nanosheets produced by liquid exfoliation of layered materials. *Science* **331**, 568 (2011). doi:10.1126/science.1194975 Medline

26. D. Teweldebrhan, A. A. Balandin, Modification of graphene properties due to electron-beam irradiation. *Appl. Phys. Lett.* **94**, 013101 (2009). doi:10.1063/1.3062851

27. I. Childres *et al*., Effect of electron-beam irradiation on graphene field effect devices. *Appl. Phys. Lett.* **97**, 173109 (2010). doi:10.1063/1.3502610